Check for updates

ADVANCING EARTH AND SPACE SCIENCES

Global Biogeochemical Cycles®

RESEARCH ARTICLE

10.1029/2023GB007843

Amplified Subsurface Signals of Ocean Acidification

Andrea J. Fassbender[1], Brendan R. Carter[1,2], Jonathan D. Sharp[1,2], Yibin Huang[1,3,4], Mar C. Arroyo[1,4], and Hartmut Frenzel[1,2]

[1]NOAA/OAR Pacific Marine Environmental Laboratory, Seattle, WA, USA, [2]Cooperative Institute for Climate, Ocean, and Ecosystem Studies, University of Washington, Seattle, WA, USA, [3]Cooperative Institute for Marine and Atmospheric Research, University of Hawai'i at Manoa, Honolulu, HI, USA, [4]Department of Ocean Sciences, University of California Santa Cruz, Santa Cruz, CA, USA

Key Points:

- The largest changes in multiple metrics of ocean acidification (OA) occur below the sea surface due to carbonate system nonlinearities
- Across broad ocean realms, subsurface changes in the partial pressure of carbon dioxide gas (pCO$_2$) driven by OA exceed the atmospheric pCO$_2$ change
- Implications for ecosystem habitability, ocean carbon storage, and marine carbon dioxide removal strategies require investigation

Supporting Information:

Supporting Information may be found in the online version of this article.

Correspondence to:

A. J. Fassbender,
andrea.j.fassbender@noaa.gov

Citation:

Fassbender, A. J., Carter, B. R., Sharp, J. D., Huang, Y., Arroyo, M. C., & Frenzel, H. (2023). Amplified subsurface signals of ocean acidification. *Global Biogeochemical Cycles*, *37*, e2023GB007843. https://doi.org/10.1029/2023GB007843

Received 13 MAY 2023
Accepted 8 NOV 2023
Corrected 14 MAR 2024

This article was corrected on 14 MAR 2024. See the end of the full text for details.

Author Contributions:

Conceptualization: Andrea J. Fassbender
Formal analysis: Andrea J. Fassbender
Methodology: Andrea J. Fassbender, Brendan R. Carter, Jonathan D. Sharp, Yibin Huang
Project Administration: Andrea J. Fassbender

© 2023 The Authors. This article has been contributed to by U.S. Government employees and their work is in the public domain in the USA.
This is an open access article under the terms of the Creative Commons Attribution License, which permits use, distribution and reproduction in any medium, provided the original work is properly cited.

Abstract We evaluate the impact of anthropogenic carbon (C_{ant}) accumulation on multiple ocean acidification (OA) metrics throughout the water column and across the major ocean basins using the GLODAPv2.2016b mapped product. OA is largely considered a surface-intensified process caused by the air-to-sea transfer of C_{ant}; however, we find that the partial pressure of carbon dioxide gas (pCO$_2$), Revelle sensitivity Factor (RF), and hydrogen ion concentration ([H$^+$]) exhibit their largest responses to C_{ant} well below the surface (>100 m). This is because subsurface seawater is usually less well-buffered than surface seawater due to the accumulation of natural carbon from organic matter remineralization. pH and aragonite saturation state (Ω_{Ar}) do not exhibit spatially coherent amplified subsurface responses to C_{ant} accumulation in the GLODAPv2.2016b mapped product, though nonlinear characteristics of the carbonate system work to amplify subsurface changes in each OA metric evaluated except Ω_{Ar}. Regional variability in the vertical gradients of natural and anthropogenic carbon create regional hot spots of subsurface intensified OA metric changes, with implications for vertical shifts in biologically relevant chemical thresholds. C_{ant} accumulation has resulted in subsurface pCO$_2$, RF, and [H$^+$] changes that significantly exceed their respective surface change magnitudes, sometimes by >100%, throughout large expanses of the ocean. Such interior ocean pCO$_2$ changes are outpacing the atmospheric pCO$_2$ change that drives OA itself. Re-emergence of these waters at the sea surface could lead to elevated CO$_2$ evasion rates and reduced ocean carbon storage efficiency in high-latitude regions where waters do not have time to fully equilibrate with the atmosphere before subduction.

Plain Language Summary The chemistry of the upper ocean is changing due to the absorption of excess carbon in the atmosphere resulting from human activities, a process commonly referred to as ocean acidification (OA). The highest concentrations of excess carbon in the ocean are generally found at the surface; however, some of the largest chemical changes resulting from this carbon buildup are occurring below the sea surface. This subsurface intensification is caused by nonlinear responses of some chemical parameters to opposing vertical gradients of natural carbon versus excess carbon. Our findings emphasize the need to study multiple metrics of OA throughout the water column to comprehensively evaluate changes in the habitability of interior ocean realms and potential connections to ocean carbon storage timescales.

1. Introduction

Anthropogenic carbon (C_{ant}) in the atmosphere is primarily transferred to the ocean through the air-sea exchange of carbon dioxide gas (CO$_2$). To date, the ocean has absorbed ~25% of the total anthropogenic emissions since industrialization (Friedlingstein et al., 2022). Persistent growth in the atmospheric partial pressure of CO$_2$ (pCO$_2$) has caused persistent growth in upper ocean C_{ant} concentrations, with the highest values generally occurring at the sea surface. However, the accumulation of C_{ant} is not spatially uniform (Gruber et al., 2019; Sabine et al., 2004). Greater penetration of C_{ant} in deep water formation regions and the subtropics is caused by regional circulation that transports surface waters to the ocean interior (DeVries, 2014; Iudicone et al., 2016; Khatiwala et al., 2013).

In addition to circulation, heterogeneity in surface ocean carbonate chemistry influences the impact of increasing atmospheric pCO$_2$ on dissolved inorganic carbon (DIC), and thus the efficiency of ocean C_{ant} accumulation (Revelle & Suess, 1957). Meridional surface gradients in temperature and salinity, in addition to physical and biological processes that can modulate local air-sea CO$_2$ disequilibrium, dictate the meridional surface gradient in DIC concentration (Hamme et al., 2019; Volk & Hoffert, 1985) and the associated DIC-to-total alkalinity ratio (Wu et al., 2019); a measure of the carbonate system buffer capacity (Egleston et al., 2010). The carbonate system

Writing – original draft: Andrea J. Fassbender
Writing – review & editing: Andrea J. Fassbender, Brendan R. Carter, Jonathan D. Sharp, Yibin Huang, Mar C. Arroyo, Hartmut Frenzel

buffer capacity is often described using the Revelle sensitivity Factor (RF; Broecker et al., 1979; Middelburg et al., 2020), which is defined as the relative change in pCO_2 associated with a relative change in DIC, assuming all other variables are held constant:

$$\mathrm{RF} = (\Delta p\mathrm{CO}_2/p\mathrm{CO}_2)(\Delta \mathrm{DIC}/\mathrm{DIC})^{-1} \tag{1}$$

For a given relative change in pCO_2, a low RF indicates that a relatively large change in DIC will occur, and a high RF indicates that a relatively small change in DIC will occur. The mean surface ocean RF is ∼10, indicating that a 10% change in pCO_2 is required to elicit a 1% change in DIC. However, spatial variability in the RF indicates that some areas of the ocean are more efficient than others at accumulating DIC for a given surface ocean pCO_2 perturbation (Figure 1a and Figure S1 in Supporting Information S1; Fassbender et al., 2017). Below the surface, the RF increases with depth, more than doubling in many ocean regions, indicating an increase in the relative sensitivity of pCO_2 to DIC (Figure 1c).

The rate at which surface ocean carbonate chemistry is changing has been well explored for a handful of ocean acidification (OA) metrics (Caldeira & Wickett, 2003; Jiang et al., 2023; Orr et al., 2005). Observation-based trends in surface ocean pCO_2 (Fay & McKinley, 2013; Jiang et al., 2023; Sutton et al., 2019; Takahashi et al., 2014), hydrogen ion concentration ($[H^+]$) (Fassbender et al., 2017; Jiang et al., 2023), pH (pH = $-\log_{10}([H^+])$; Iida et al., 2021; Jiang et al., 2019, 2023; Lauvset et al., 2015), and the saturation state of aragonite (Ω_{Ar}: a calcium carbonate mineral polymorph; Bates et al., 2014; Feely et al., 2009; Iida et al., 2021) have been evaluated globally. Less attention has been given to carbonate chemistry changes occurring in the ocean interior where vertical DIC gradients greatly exceed horizontal DIC gradients across the open surface ocean (Figures 1b and 1d). Exceptions include a few global studies that have evaluated subsurface changes in calcium carbonate mineral saturation states and pH (Feely et al., 2004; Jiang et al., 2015; S. K. Lauvset et al., 2020) and regional studies that have evaluated subsurface changes in pCO_2 (Arroyo et al., 2022; Chen et al., 2022), $[H^+]$ (Arroyo et al., 2022; Fassbender et al., 2021), pH (Arroyo et al., 2022; Byrne et al., 2010; Carter et al., 2019; Chen et al., 2017; Dore et al., 2009; Fassbender et al., 2021), and aragonite saturation state (Ω_{Ar}) (Arroyo et al., 2022; Carter et al., 2019; Feely et al., 2018; Negrete-García et al., 2019). Some of these studies suggest that the largest OA metric responses to C_{ant} may be occurring below the sea surface (Arroyo et al., 2022; Carter et al., 2019; Fassbender et al., 2021; Lauvset et al., 2020).

In the ocean interior, the three-dimensional habitats of marine species are shaped by environmental conditions (e.g., Deutsch et al., 2020; Howard et al., 2020) that evolve with natural variability and external forcing. Yet, few studies have evaluated how OA metrics influence the distributions of economically important species and their prey (e.g., Guinotte & Fabry, 2008). For example, Ω_{Ar} is a valuable indicator of the energetic requirement to sustain net calcification (e.g., Bach, 2015) for species that may serve as prey for pelagic fish or be economically important in their own right (Cooley & Doney, 2009). Additionally, there is evidence that some fish species may be severely impacted by elevated seawater pCO_2 levels that can make it difficult to expel CO_2 from the gills, causing a buildup of CO_2 in the blood (i.e., hypercapnia; Heuer & Grosell, 2014). Understanding how OA is evolving below the surface, where new mesopelagic fisheries may become important to feed the growing global population (Fjeld et al., 2023; Kourantidou & Jin, 2022), is a critical first step toward identifying potential downstream impacts of OA on marine species distributions and ecosystem health.

Building on prior studies, we evaluate the impact of C_{ant} accumulation on multiple commonly considered OA metrics throughout the water column and across the major ocean basins. We then quantify the impact of carbonate system nonlinearities on the C_{ant}-induced OA metric changes. The indirect impacts of C_{ant} on ocean circulation and the biological carbon pump through climate change are additional complications that we do not address in this study. Finally, we consider potential implications for interior ocean habitability, carbon storage efficiency, and impacts resulting from marine carbon dioxide removal strategies.

2. Methodology

2.1. OA Metric Changes Caused by C_{ant}

To quantify the impact of C_{ant} on each OA metric (i.e., pH, Ω_{Ar}, pCO_2, $[H^+]$, and RF), we rely on a quality-controlled and internally consistent hydrographic data set curated by the Global Data Analysis Project (GLODAP; Olsen et al., 2016) that was previously mapped to a global 1° × 1° horizontal grid with 33 stand-

19449224, 2023, 12, Downloaded from https://agupubs.onlinelibrary.wiley.com/doi/10.1029/2023GB007843 by Ifremer Centre Bretagne Blp, Wiley Online Library on [06/03/2025]. See the Terms and Conditions (https://onlinelibrary.wiley.com/terms-and-conditions) on Wiley Online Library for rules of use; OA articles are governed by the applicable Creative Commons License

19449224, 2023, 12, Downloaded from https://agupubs.onlinelibrary.wiley.com/doi/10.1029/2023GB007843 by Ifremer Centre Bretagne Blp, Wiley Online Library on [06/03/2025]. See the Terms and Conditions (https://onlinelibrary.wiley.com/terms-and-conditions) on Wiley Online Library for rules of use; OA articles are governed by the applicable Creative Commons License

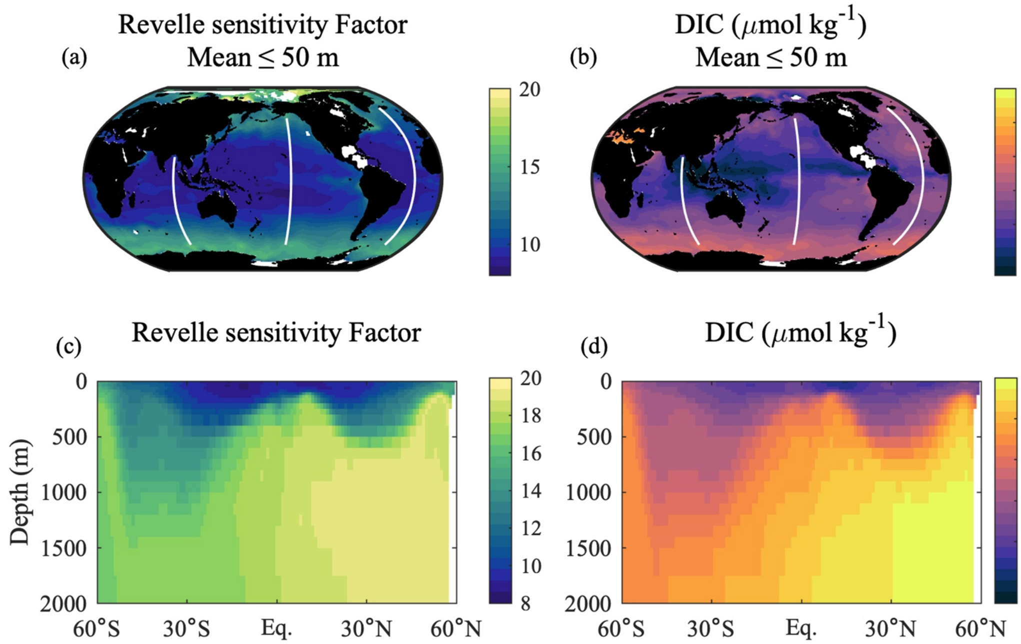

Figure 1. Average (a) Revelle sensitivity Factor (RF) and (b) dissolved inorganic carbon (DIC) concentration in the upper 50 m of the ocean. Interior ocean (c) RF and (d) DIC concentrations along 150.5°W (central white line in panels (a) and (b)). Panels a and c as well as b and d use consistent color scales to emphasize the larger interior ocean versus near-surface gradients in these parameters. Data are from the GLODAPv2.2016b mapped product, which is an annual climatology normalized to the year 2002 (Lauvset et al., 2016). White patches in panels (a) and (b) reflect regions lacking data. Panels (a) and (b) also show meridional transects (white lines) in the Atlantic (25.5°W) and Indian (90.5°E) Oceans that will be referenced in subsequent figures.

ard depth levels and normalized to the year 2002 as an annual climatology: the GLODAPv2.2016b mapped product (Key et al., 2015; Lauvset et al., 2016). Salinity (*S*), temperature (*T*), total alkalinity (TA), DIC, and nutrient (N; phosphate and silicate) data were used to compute pH, Ω_{Ar}, pCO_2, $[H^+]$, and RF (Figure S2 in Supporting Information S1). All carbonate system calculations in our study were made in MATLAB using the CO2SYSv3 (version 3.2.0; Sharp et al., 2020) carbonate system calculator with the following user settings: total pH scale; equilibrium constants of Lueker et al. (2000); sulfate dissociation constant of Dickson et al. (1990); fluoride dissociation constant of Perez and Fraga (1987); and borate-to-salinity ratio of Lee et al. (2010).

C_{ant} values included in the GLODAPv2.2016b mapped product were subtracted from the DIC values to estimate a quasi-preindustrial (PI) DIC concentration (DIC_{PI}). The GLODAPv2.2016b mapped product does provide a DIC_{PI} field, but it is mapped from calculations of DIC_{PI} at observation locations and is nearly identical (0.0 ± 0.2 μmol kg^{-1}) to the mapped DIC minus mapped C_{ant}. We chose to deal with DIC_{PI} calculated from the mapped DIC and C_{ant} for consistency. Salinity, temperature, TA, DIC_{PI}, and nutrient data were then used to compute pH_{PI}, $\Omega_{Ar\ PI}$, $pCO_{2\ PI}$, $[H^+]_{PI}$, and RF_{PI}. This approach isolates the influence of accumulated C_{ant} in setting ocean chemical conditions (in 2002 c.e.) but does not account for changes in temperature, salinity, ocean circulation, or biology that may have occurred since industrialization. Differences between the year 2002 and PI values are used to evaluate subsurface patterns of OA metric changes caused by accumulated C_{ant} (for a variable X this would be $\Delta X^{C_{ant}}$; Figure S3 in Supporting Information S1), with an example calculation for pH shown here:

$$\Delta pH^{C_{ant}} = pH^{f(S,T,DIC,TA,N)} - pH_{PI}^{\ f(S,T,DIC_{PI},TA,N)} \quad (2)$$

We consider subsurface changes in each OA metric relative to the respective mean change within the upper 50 m of the local overlying water ($\Delta pH^{C_{ant}} - \overline{\Delta pH^{C_{ant}}}|_{0-50m}$). Local overlying waters do not typically reflect the origin conditions of the waters below; however, using the local, rather than global, mean change in near-surface waters as a reference helps to reveal how the influence of this feedback varies with depth (Figures S4 and S5 in Supporting Information S1).

2.2. Nonlinear Component of OA Metric Changes Caused by C_{ant}

To quantify how carbonate system nonlinearities may be contributing to the total change in each OA metric, we use previously published, globally mapped estimates of preformed properties (Carter et al., 2021) provided on the same grid as the GLODAPv2.2016b mapped product. These so-called preformed properties reflect the property concentrations that would be expected in the absence of carbon accumulated through organic matter remineralization (Figure S6 in Supporting Information S1) and calcium carbonate dissolution (Figure S7 in Supporting Information S1). The interior ocean preformed property estimates rely on the transport matrix output from a data-assimilation ocean circulation inverse model (OCIM: DeVries, 2014) to determine where interior ocean water masses were last near the ocean surface, and two alternative circulation products are used as a component of the uncertainty estimate for the product. OCIM in turn relies on GLODAP observations (Key et al., 2004) of potential temperature, salinity, radiocarbon, and CFC-11 to estimate the climatological mean state ocean circulation. Locally interpolated regression algorithms developed by Carter et al. (2017), which are also based on GLODAP observations, were used to estimate preformed property values at the base of the mixed layer. These values were propagated into the ocean interior using the OCIM transport matrix to estimate the interior ocean preformed property values. As a final step, Carter et al. (2021) regridded the preformed properties to match the GLODAPv2.2016b mapped product grid for public release of the files.

We focus on the biogenic component of natural carbon in the ocean due to its dominance in setting the vertical carbon gradient (DeVries, 2022; Sarmiento & Gruber, 2006) and because it is the addition of biogenic carbon, after natural and anthropogenic carbon have been added through air-sea exchange, that induces the nonlinear subsurface changes we aim to characterize (Figure S8 in Supporting Information S1). We subtract the preformed dissolved oxygen ($O_{2\,0}$) field from the GLODAPv2.2016b mapped product O_2 field to estimate the true oxygen utilization (TOU). To convert TOU to respiratory DIC, we use the canonical respiratory quotient (O_2:C) of (−170/117) that was estimated from mixed phytoplankton tows (Hedges et al., 2002) and interior ocean water mass analyses (Anderson & Sarmiento, 1994) to evaluate the bulk remineralized carbon pool in the ocean interior (sensitivity analysis presented in Text S1 and Figures S9–S10 in Supporting Information S1). We subtract preformed nitrate, silicate, and phosphate from the GLODAPv2.2016b mapped product fields for each parameter to determine their respiratory burdens. Following Carter et al. (2021), we compute potential alkalinity (*p*TA) by subtracting the GLODAPv2.2016b mapped product nitrate field multiplied by 1.36 (Wolf-Gladrow et al., 2007) from the TA field to account for the minor influence of remineralization on TA. We perform the same calculation using the preformed TA (TA_0) and preformed nitrate fields to estimate preformed potential TA (pTA_0). The difference between pTA and pTA_0 yields the calcium carbonate dissolution term (TA_{CaCO3}). Subtracting TA_0 and TA_{CaCO3} from the TA field yields the residual, remineralized TA component. We multiply TA_{CaCO3} by 0.5 to calculate the DIC calcium carbonate dissolution component. Preformed DIC (DIC_0) is then calculated by subtracting the respiratory and calcium carbonate DIC components from the GLODAPv2.2016b mapped product DIC field.

For each OA metric, the preindustrial preformed (PI,0) value is subtracted from the year 2002 preformed value to determine OA metric changes $\left(\Delta X_0^{C_{ant}}\right)$ in the absence of natural biogenic byproducts, with an example calculation for pH shown here:

$$\Delta pH_0{}^{C_{ant}} = pH_0{}^{f(S,T,DIC_0,TA_0,N_0)} - pH_{PI,0}{}^{f(S,T,DIC_{PI,0},TA_0,N_0)} \tag{3}$$

For each OA metric (e.g., X), we then evaluate the difference between C_{ant}-induced changes occurring with ($\Delta X^{C_{ant}}$) and without ($\Delta X_0^{C_{ant}}$) the background of natural biogenic carbon byproducts (hereafter referred to as natural carbon). This allows us to quantify how much of the OA metric response is caused by nonlinear carbonate chemistry effects induced by natural and anthropogenic carbon pool interactions (Figure S8 in Supporting Information S1), with an example calculation for pH shown here:

$$\Delta pH_{Nonlinear} = \Delta pH^{C_{ant}} - \Delta pH_0{}^{C_{ant}} \tag{4}$$

In the history of a water mass, C_{ant} accumulates before and during water mass formation and subduction, whereas natural carbon accumulates after water mass subduction. Therefore, this nonlinear effect should be considered the impact of C_{ant} upon the magnitude of change induced by natural carbon rather than the reverse. Nevertheless, hereafter we discuss the impact in the reverse sense because we are interested in how human emissions modulate the signals associated with natural environmental variability.

19449224, 2023, 12, Downloaded from https://agupubs.onlinelibrary.wiley.com/doi/10.1029/2023GB007843 by Ifremer Centre Bretagne Blp, Wiley Online Library on [06/03/2025]. See the Terms and Conditions (https://onlinelibrary.wiley.com/terms-and-conditions) on Wiley Online Library for rules of use; OA articles are governed by the applicable Creative Commons License

19449224, 2023, 12, Downloaded from https://agupubs.onlinelibrary.wiley.com/doi/10.1029/2023GB007843 by Ifremer Centre Bretagne Blp, Wiley Online Library on [06/03/2025]. See the Terms and Conditions (https://onlinelibrary.wiley.com/terms-and-conditions) on Wiley Online Library for rules of use; OA articles are governed by the applicable Creative Commons License

Our calculations rely on numerous assumptions and data products, each of which contains a degree of uncertainty. However, in Text S2, we describe a validation exercise based on independent output from a global ocean biogeochemistry model that reproduces the significant patterns that we highlight in our findings (Figure S11 in Supporting Information S1). This confirms that our findings are not spurious products of our methodological choices but are robust signals that are consistent with modern understanding of ocean circulation, biogeochemistry, and anthropogenic forcing. While this exercise shows that models already represent subsurface amplification of OA metric changes through carbonate system nonlinearities, our study serves to characterize and to call attention to this combination of unintuitive feedbacks and to provide observational evidence for its existence and extent in the real ocean.

2.3. Estimation of Uncertainties

The GLODAPv2.2016b mapped product provides spatially resolved error fields for each parameter. These errors reflect mapping uncertainties and do not include measurement uncertainties or calculation errors (for pH and Ω_{Ar}), as mapping errors are thought to dominate (Lauvset et al., 2016; Olsen et al., 2016). We compute the [H^+] error directly from the provided pH and pH_{error} fields (Text S3). The Carter et al. (2021) preformed a property mapped product also provides spatially resolved error fields for each parameter. We use the error fields in Monte Carlo simulations and standard error propagation procedures (i.e., summing in quadrature) to estimate the uncertainty in the calculated values presented herein. For pCO_2, RF, and all PI values, we perform a 1,000 iteration Monte Carlo simulation of the CO2SYSv3 calculations while individually varying all input values around their provided errors in a Gaussian manner using a MATLAB pseudorandom number generator (randn) that produces a set of numbers with a mean equal to zero and standard deviation equal to one. We also calculate the change in each parameter from the PI period to the year 2002 within each simulation. The standard deviation across the 1,000 simulations for each parameter is used to estimate its uncertainty. Standard error propagation is used in subsequent calculations as needed. The computed uncertainties are used for stippling in various figures to convey statistical confidence.

3. Results

3.1. Identifying OA Metrics With Subsurface Intensified Changes

pH and Ω_{Ar} do not display coherent, amplified subsurface C_{ant}-induced changes $\left(\Delta X^{C_{ant}}\right)$ relative to the local mean changes within the upper 50 m along the transects evaluated (Figure 2 and Figure S12 in Supporting Information S1). However, there are patchy regions of slightly elevated subsurface $\Delta pH^{C_{ant}}$ that exceed the calculation uncertainties (Figures 2a–2c), and similar signals have been identified previously (Carter et al., 2019; Lauvset et al., 2020). pCO_2 and [H^+] display amplified subsurface C_{ant}-induced changes, relative to the local mean changes within the upper 50 m, with the largest changes occurring at depths with moderate to low C_{ant} concentrations (Figure 2 and Figure S12 in Supporting Information S1). These features are spatially coherent and found throughout significant portions of each ocean transect, reflecting a signal that is global in nature. The largest subsurface $\Delta pCO_2^{C_{ant}}$ and $\Delta\left[H^+\right]^{C_{ant}}$ signals occur in the North Pacific (~100–500 m) where the waters are old (Figure S13 in Supporting Information S1), the vertical pCO_2 and DIC gradients are steep (Figure S14 in Supporting Information S1), and carbonate system buffering is naturally weak (Figure 1c). In these areas, small changes in DIC have a large influence on pCO_2 due to the elevated background pCO_2:DIC ratio (Figure S15a in Supporting Information S1; Equation 1; Fassbender et al., 2017). Similarly large subsurface $\Delta pCO_2^{C_{ant}}$ and $\Delta\left[H^+\right]^{C_{ant}}$ signals are found in the North Indian Ocean where C_{ant} penetration is shallow but the vertical pCO_2:DIC gradient is also shallow and steep (Figure S14 in Supporting Information S1). In the North Atlantic and Southern Oceans, where C_{ant} reaches deep into the interior, weaker vertical carbon gradients in the more recently ventilated waters cause subsurface $\Delta pCO_2^{C_{ant}}$ and $\Delta\left[H^+\right]^{C_{ant}}$ signals to exceed the near-surface changes by a much smaller magnitude. Larger GLODAPv2.2016b mapped product uncertainties in the Southern Ocean, due to data scarcity (Lauvset et al., 2016), cause most of the $\Delta\left[H^+\right]^{C_{ant}}$ signals in this region to fall within the uncertainties of the calculation.

Like pCO_2 and [H^+], the RF exhibits amplified subsurface C_{ant}-induced changes relative to the local mean changes within the upper 50 m, with the largest changes occurring at depths with moderate to low C_{ant} concentrations (Figure 2). Poleward of ~45°N in the Pacific Ocean, there is a large discrepancy in the vertical extent of subsurface $\Delta RF^{C_{ant}}$ versus $\Delta pCO_2^{C_{ant}}$ signals (Figure S3 in Supporting Information S1). These waters surpassed their minimum buffer capacity (or maximum RF) in the preindustrial ocean (Figures S12 and S16 in Supporting Information S1), such that the addition of C_{ant} causes $\Delta RF^{C_{ant}}$ to be negative (Egleston et al., 2010; Fassbender

10.1029/2023GB007843

19449224, 2023, 12, Downloaded from https://agupubs.onlinelibrary.wiley.com/doi/10.1029/2023GB007843 by Ifremer Centre Bretagne Blp, Wiley Online Library on [06/03/2025]. See the Terms and Conditions (https://onlinelibrary.wiley.com/terms-and-conditions) on Wiley Online Library for rules of use; OA articles are governed by the applicable Creative Commons License

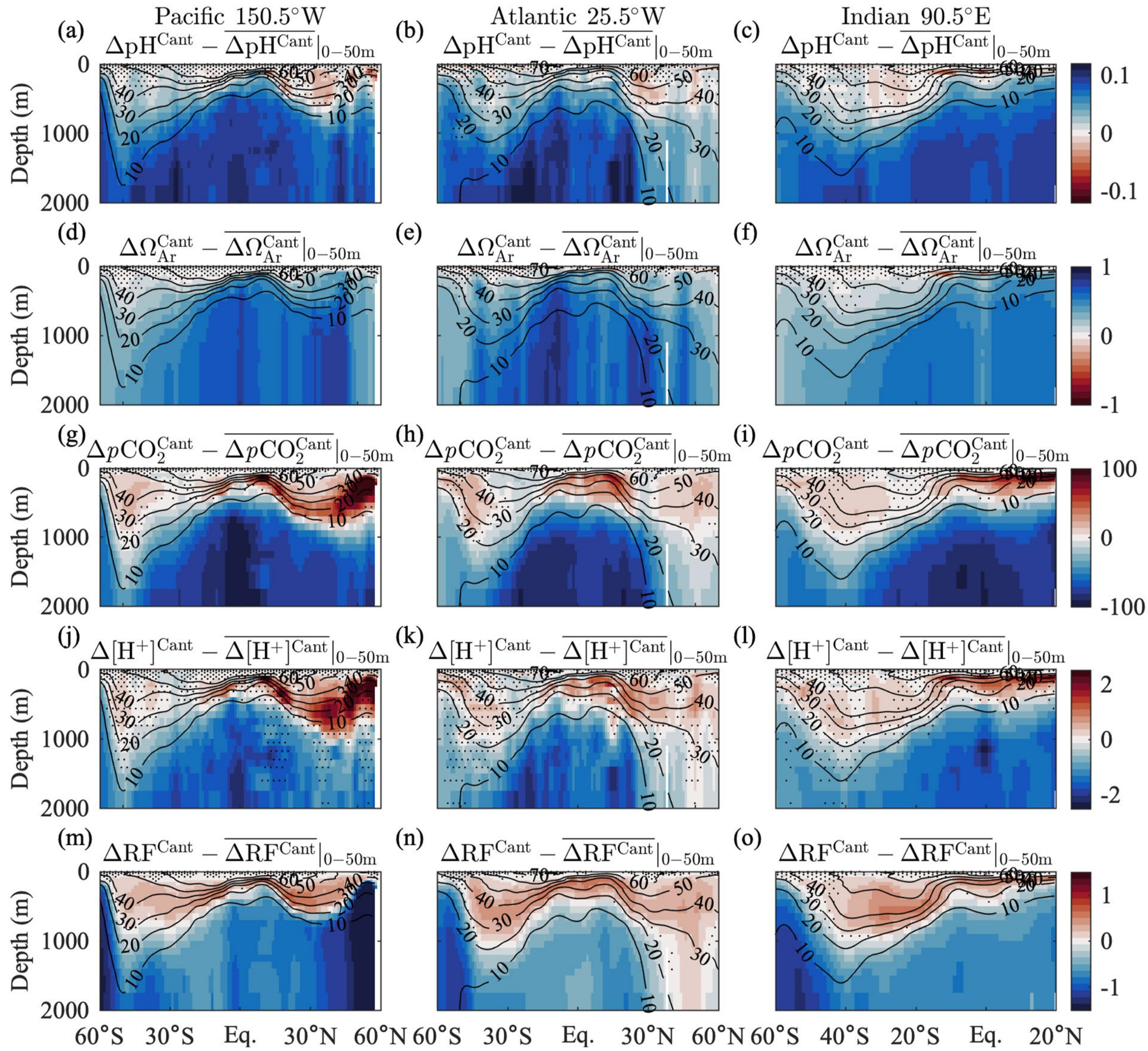

Figure 2. C_{ant}-induced ocean acidification metric changes (Δ), from the preindustrial period to the year 2002, relative to the local mean change in the upper 50 m for (a–c) pH, (d–f) aragonite saturation state (Ω_{Ar}), (g–i) partial pressure of carbon dioxide gas (pCO$_2$; μatm), (j-l) [H$^+$] (nmol kg^{-1}), and the (m–o) Revelle sensitivity Factor. Results for the Pacific (150.5°W), Atlantic (25.5°W), and Indian (90.5°E) Oceans with meridional transect locations shown in Figure 1a. Black contours represent C_{ant} (μmol kg^{-1}) in the year 2002. Red coloring indicates a subsurface change that is larger in magnitude than the local mean change in the upper 50 m. Stippling indicates where the magnitude of the change is smaller than the uncertainty.

et al., 2017). The maximum RF is found where DIC approximately equals TA (Figure S15b in Supporting Information S1). Where DIC < TA, as it is in much of the modern ocean, the RF increases with DIC additions, as carbonate ions are consumed to neutralize the added CO_2 (Figure S15c in Supporting Information S1), thus diminishing the quantity of carbonate ions remaining to buffer the seawater against further changes. When DIC > TA, the carbonate ions have been largely consumed, leading to an approximately linear increase in pCO_2 with increasing DIC (Figures S15a and S15c in Supporting Information S1). In these regions, the RF declines with added DIC, primarily due to a constant $\Delta pCO_2/\Delta$DIC and rapidly growing pCO_2 denominator in Equation 1. Like pCO_2, subsurface $\Delta \mathrm{RF}^{C_{ant}}$ values throughout the Southern Ocean are larger than the uncertainties (Figures 2m–2o).

3.2. Nonlinear Interactions Between Natural and Anthropogenic Carbon Pools

Regional differences in vertical DIC and TA gradients caused by heterogeneous accumulation of biogenic and anthropogenic carbon (Figures S6 and S7 in Supporting Information S1) lead to regional differences in the nonlinear responses of OA metrics to natural and anthropogenic carbon pool interactions (Figure 3). Ocean C_{ant} distributions

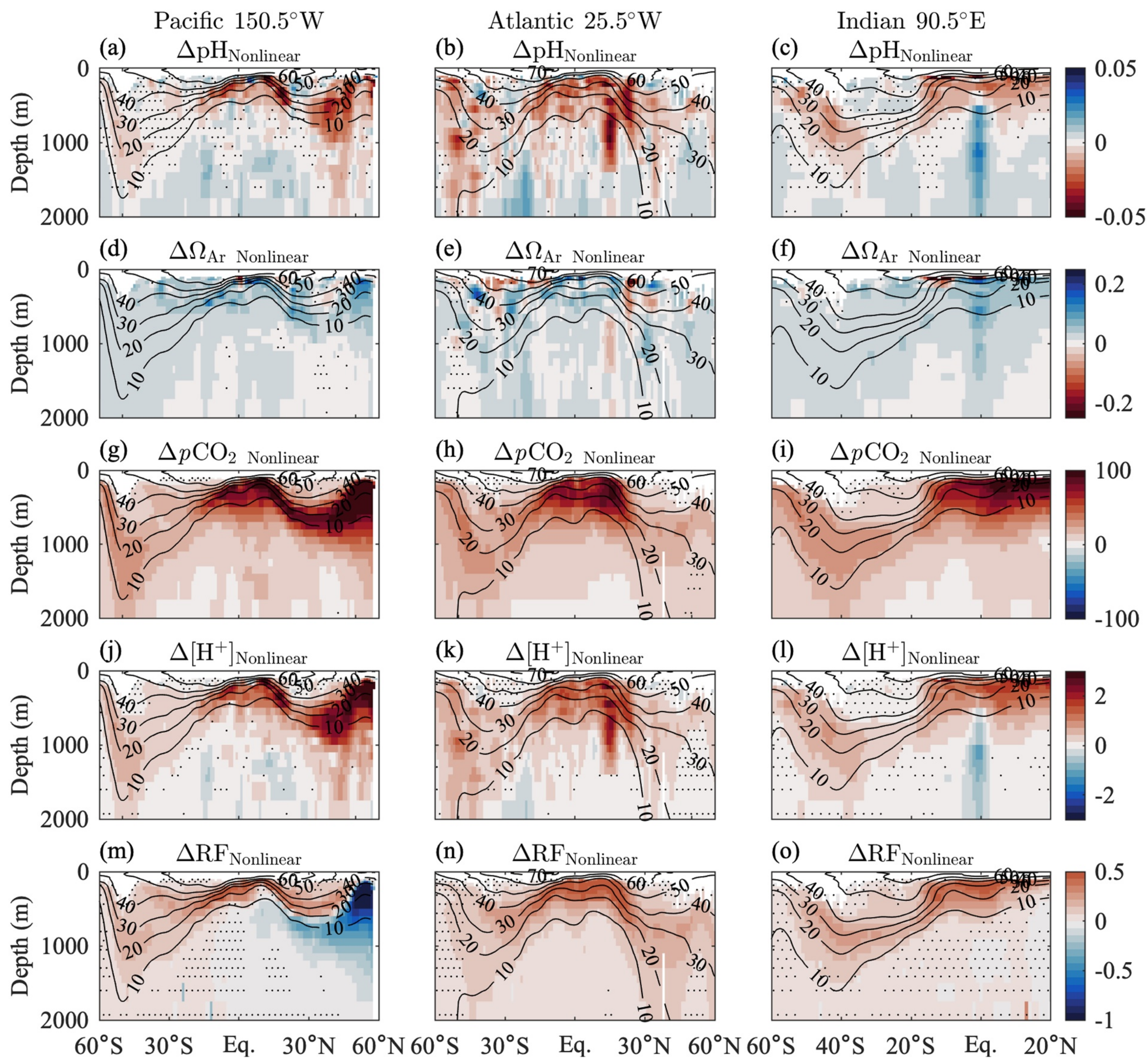

Figure 3. Nonlinear component of ocean acidification (OA) metric changes (Δ) caused by interactions between C_{ant} and natural carbon accumulated from organic matter remineralization and calcium carbonate dissolution. Red and blue coloring indicate where the OA metric responses to C_{ant} are amplified or dampened, respectively, by carbonate system nonlinearities. Results are shown for (a–c) pH (d–f) aragonite saturation state (Ω_{Ar}), (g–i) partial pressure of carbon dioxide gas (pCO$_2$; μatm), (j-l) [H$^+$] (nmol kg^{-1}), and the (m-o) Revelle sensitivity Factor. Black contours represent C_{ant} (μmol kg^{-1}) in the year 2002. Results for the Pacific (150.5°W), Atlantic (25.5°W), and Indian (90.5°E) Oceans with meridional transect locations shown in Figure 1a. Stippling indicates where the magnitude of the change is smaller than the uncertainty.

reflect the uptake of a non-steady-state tracer sourced from the atmosphere and the passive redistribution of this surface signal into the ocean interior through ocean circulation. Biogeochemical feedback also have the potential to impact C_{ant} distributions, but the transient-tracer-based transit-time C_{ant} distribution estimates used in this study do not capture or represent these secondary controls on C_{ant} distributions. By contrast, vertical gradients in natural carbon primarily result from biological processes and are only secondarily controlled by the temperature-driven CO_2 solubility prior to water mass subduction (i.e., the solubility pump) (Figure S6 in Supporting Information S1). Importantly, natural carbon tends to increase with water mass age while C_{ant} tends to decrease with water mass age. This leads to a decoupling of large-scale C_{ant} and natural carbon gradients along neutral density surfaces, creating hotspots for the emergence of nonlinear carbonate chemistry signals in the ocean interior.

Nonlinear interactions between natural and anthropogenic carbon pools are working to both dampen and amplify OA metric changes in different regions of the water column. For pH, nonlinearities amplify the decrease in pH throughout coherent regions of the subsurface ocean (Figure 3); however, this effect is small, accounting for <25% of the

19449224, 2023, 12, Downloaded from https://agupubs.onlinelibrary.wiley.com/doi/10.1029/2023GB007843 by Ifremer Centre Bretagne Blp, Wiley Online Library on [06/03/2025]. See the Terms and Conditions (https://onlinelibrary.wiley.com/terms-and-conditions) on Wiley Online Library for rules of use; OA articles are governed by the applicable Creative Commons License

10.1029/2023GB007843

total pH change in waters above the 10 μmol kg^{-1} C_{ant} contour (Figure S17 in Supporting Information S1), where pH changes are greatest. As a result, nonlinear pH changes are not large enough to produce a coherent, elevated subsurface signal in the overall pH change or in the pH change relative to the upper 50 m in the GLODAPv2.2016b mapped product (Figure 2 and Figure S3 in Supporting Information S1). Model estimates of interior ocean nonlinear pH changes caused by C_{ant} accumulation (Figure S11 and Text S2 in Supporting Information S1) imply that subsurface amplified signals may be anticipated but are difficult to detect amid uncertainties in the underlying observational products. For Ω_{Ar}, carbonate system nonlinearities dampen the decrease in Ω_{Ar} throughout the water column, but the effect is small, accounting for <25% of the total Ω_{Ar} change in most waters above the 10 μmol kg^{-1} C_{ant} contour (Figure S17), where Ω_{Ar} changes are greatest (Figure S3 in Supporting Information S1). Carbonate system nonlinearities work to significantly increase pCO_2 and [H$^+$] changes below the surface, accounting for >70% of the total changes in waters laden with respiratory byproducts above the 10 μmol kg^{-1} C_{ant} contour, where changes in these parameters are greatest (Figures S3, S6, and S17 in Supporting Information S1). For the RF, nonlinear contributions to the OA driven changes are predominantly small (<35% of the total RF change), excluding a large dampening signal in the mesopelagic North Pacific that is entirely explained by carbonate system nonlinearities (Figure S17 in Supporting Information S1). In this region the preindustrial DIC:TA ratio is already greater than 1 and increases in DIC from C_{ant} accumulation lead to declines in the RF (Figure S16 in Supporting Information S1). However, adding C_{ant} to the preformed PI values, for which the DIC:TA ratio is much less than 1, causes the RF to increase. Differencing these changes (Equation 4) leads to the large nonlinear reduction in the RF. In summary, carbonate system nonlinearities resulting from natural and anthropogenic carbon pool interactions mitigate C_{ant}-driven changes to Ω_{Ar} and exacerbate changes to pH, pCO_2, and [H$^+$] in coherent spatial patterns. The RF responds similarly to pCO_2 in regions where the DIC:TA ratio remains <1 (Figures S3 and S16 in Supporting Information S1).

3.3. Potential Implications for Habitat Compression

The largest [H$^+$] and pCO_2 changes resulting from accumulated C_{ant} in the open ocean have occurred below the sea surface (Figure 2) in mesopelagic waters where organisms are also experiencing reductions in carbonate mineral saturation (Jiang et al., 2015) and dissolved oxygen levels (hypoxia; $O_2 \leq 60$ μmol kg^{-1}; Breitburg et al., 2018; Oschlies et al., 2018). Elevated in situ pCO_2 has been linked to negative impacts for a suite of sessile and low-vagility invertebrates (Vargas et al., 2022), and there is mixed evidence for adverse impacts on marine fishes through several biological mechanisms (Clements & Hunt, 2015; Esbaugh, 2018; Heuer & Grosell, 2014; Sundin, 2023). One of these mechanisms is a reduction in the efficiency at which CO_2 is expelled during respiration, which can lead to a buildup of CO_2 in the blood (i.e., hypercapnia; Nilsson et al., 2012; Perry & Gilmour, 2006). 1,000 μatm is commonly used as a pCO_2 threshold for when respiring marine organisms may experience stress (Arroyo et al., 2022; Feely et al., 2018; McNeil & Sasse, 2016).

The interior ocean pCO_2 we have presented until now reflects the partial pressure that CO_2 would have if it were an ideal gas that was unaffected by the overlying hydrostatic pressure. This is a useful parameter for considering the air-sea pCO_2 gradient that would occur if subsurface waters were instantaneously and quasi-adiabatically brought to the sea surface where pCO_2 and the fugacity of CO_2 (fCO_2) are quite similar (Humphreys et al., 2022). However, in the ocean interior, the influence of overlying pressure and non-ideal nature of CO_2 may be an important consideration (Figure S18 in Supporting Information S1). Thus, we compute in situ fCO_2 values (Text S4) and evaluate hypercapnia (hereafter equating to $fCO_2 \geq 1{,}000$ μatm) in the ocean interior and its relation to patterns of low oxygen and Ω_{Ar}.

Hypercapnic conditions can be found at depths shallower than 500 m throughout large expanses of the Pacific Ocean as well as the Bay of Bengal, Arabian Sea, and off the west coast of Africa (Figure 4a). C_{ant}-driven fCO_2 increases in the ocean interior have contributed to this signal, causing widespread shoaling of the hypercapnia horizon (~180 m along the Pacific transect; green vs. purple line in Figure 4c). A significant volume of hypercapnic water in the Eastern Equatorial Pacific, North Pacific Ocean, and North Indian Ocean is also hypoxic (Figure 4b). In the North Pacific, the hypoxia and hypercapnia horizons closely align with the aragonite saturation horizon at depths ≤200 m (Figure 4d).

4. Discussion

4.1. Amplified Subsurface Ocean Acidification

OA caused by the air-to-sea transfer of C_{ant} is intuitively thought to be a surface-intensified process, but this is not the case across broad ocean regions and for multiple OA metrics, including pCO_2, RF, and [H$^+$]. By the

19449224, 2023, 12, Downloaded from https://agupubs.onlinelibrary.wiley.com/doi/10.1029/2023GB007843 by Ifremer Centre Bretagne Blp, Wiley Online Library on [06/03/2025]. See the Terms and Conditions (https://onlinelibrary.wiley.com/terms-and-conditions) on Wiley Online Library for rules of use; OA articles are governed by the applicable Creative Commons License

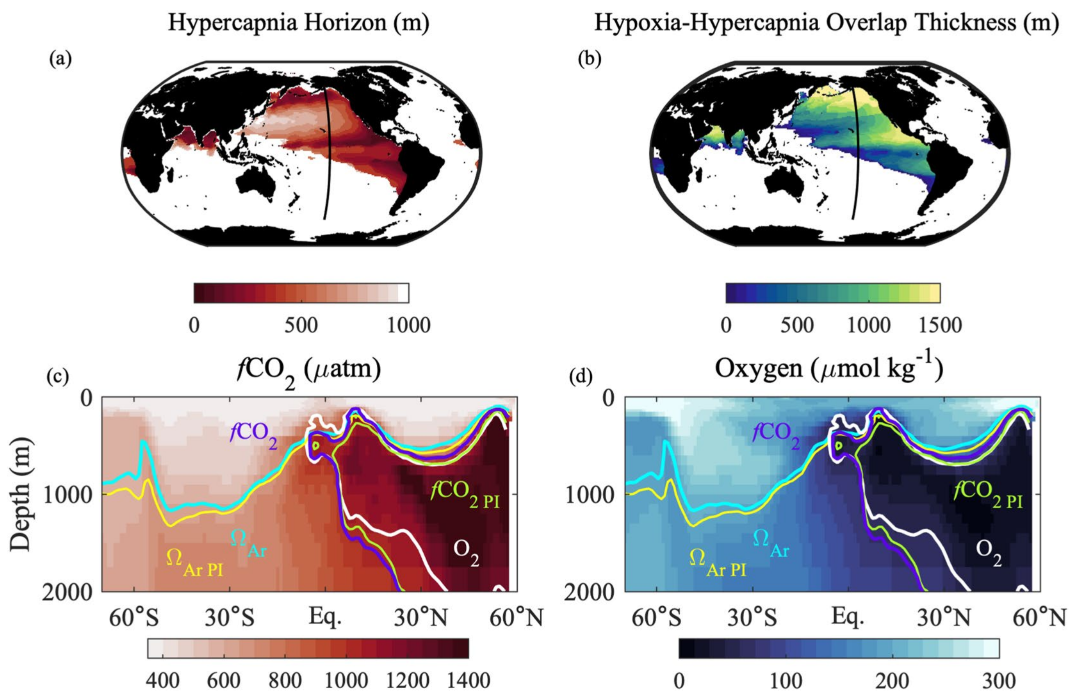

Figure 4. Year 2002 (a) depth of the hypercapnia horizon (fCO_2 = 1,000 µatm) and (b) thickness of overlap in simultaneously hypercapnic and hypoxic ($O_2 \leq 60$ µmol kg^{-1}) waters. (c) Year 2002 fCO_2 and (d) dissolved oxygen concentration along North Pacific Section 150.5°W. Purple and green lines show the year 2002 and PI hypercapnia horizons (fCO_2), respectively. Cyan and yellow lines show the year 2002 and PI aragonite saturation horizons (Ω_{Ar}), respectively. White lines show the year 2002 hypoxia horizon (O_2).

year 2002, these parameters exhibited their largest responses to C_{ant} accumulation in the ocean interior, where waters are weakly buffered due to the buildup of remineralized organic material, and C_{ant} concentrations are moderate. Annual mean surface ocean pCO_2 growth largely tracks atmospheric pCO_2 growth, globally and over multi-decadal timescales (McKinley et al., 2017), increasing by ~90 µatm from the PI to the year 2002 (Figure S1b in Supporting Information S1). Subsurface $\Delta pCO_2^{C_{ant}}$ values that exceed the upper 50 m mean $\Delta pCO_2^{C_{ant}}$ value (Figure 2) are therefore outpacing the atmospheric pCO_2 perturbation, more than doubling it in some regions of the North Pacific and North Indian Oceans. This is particularly notable since these waters reside below the local maximum annual mixed layer depth and have not been in contact with the atmosphere for some time (Figure S13 in Supporting Information S1).

Aragonite saturation state does not exhibit a subsurface intensified response to C_{ant} accumulation while pH exhibits an inconsistent subsurface intensified response to C_{ant} accumulation in the GLODAPv2.2016b mapped product. There are patches of slightly elevated C_{ant}-driven pH changes below the surface that exceed our calculation uncertainties, and the model analysis (Text S2) indicates that carbonate system nonlinearities are working to induce widespread subsurface pH change amplification (Figure S11 in Supporting Information S1). pH changes reflect relative [H$^+$] changes (Fassbender et al., 2021; Kwiatkowski & Orr, 2018), so small positive biases in the 2002 subsurface [H$^+$] values or negative biases in the C_{ant} estimates (which would cause negative biases in $\Delta[H^+]^{C_{ant}}$) could be muting the large-scale $\Delta pH^{C_{ant}}$ signal and causing the small and localized subsurface $\Delta pH^{C_{ant}}$ minima that we find. Alternatively, these patches could reflect unaccounted for uncertainties associated with mapping C_{ant} and/or pH to a global scale to create the GLODAPv2.2016b mapped product. We find that carbonate system nonlinearities are working to amplify the subsurface responses of pCO_2, RF, [H$^+$], and pH to C_{ant} accumulation, dominating the overall responses of pCO_2 and [H$^+$] as well as the response of RF in some ocean regions. Continued OA may cause the patchy $\Delta pH^{C_{ant}}$ minima to expand into coherent subsurface signals like those found in a recent analysis of 21st century Earth system model projections (Kwiatkowski et al., 2020). Nonlinear carbonate chemistry effects weakly mitigate reductions in Ω_{Ar}, which has a surface intensified response to C_{ant} accumulation. Our findings therefore do not add significant new context to C_{ant}-driven Ω_{Ar} changes relative to previous interior ocean analyses (e.g., Feely et al., 2004; Negrete-García et al., 2019).

19449224, 2023, 12, Downloaded from https://agupubs.onlinelibrary.wiley.com/doi/10.1029/2023GB007843 by Ifremer Centre Bretagne Blp, Wiley Online Library on [06/03/2025]. See the Terms and Conditions (https://onlinelibrary.wiley.com/terms-and-conditions) on Wiley Online Library for rules of use; OA articles are governed by the applicable Creative Commons License

19449224, 2023, 12, Downloaded from https://agupubs.onlinelibrary.wiley.com/doi/10.1029/2023GB007843 by Ifremer Centre Bretagne Blp, Wiley Online Library on [06/03/2025]. See the Terms and Conditions (https://onlinelibrary.wiley.com/terms-and-conditions) on Wiley Online Library for rules of use; OA articles are governed by the applicable Creative Commons License

4.2. Broader Implications

The OA metrics evaluated herein are not routinely incorporated into marine ecosystem models, which are forced with output from Earth system model projections to estimate future ocean biomass changes (Doney et al., 2020; Lotze et al., 2019; Tittensor et al., 2021). However, there is growing interest to understand how climate change, including OA, is impacting the marine environment, and to use this understanding to support ecosystem-based fishery management (Edited by In Bianchi & Skjoldal, 2008; Fletcher et al., 2010; Garcia & Cochrane, 2005; Marshall et al., 2019; Pikitch et al., 2004). A large body of experimental OA work suggests that species from more variable marine environments tend to have more phenotypic plasticity and are thus more tolerant of environmental variability (Boyd et al., 2016). However, most biological OA sensitivity studies use modern or preindustrial near-surface ocean conditions as a baseline mean state from which to conduct their experimental treatments (e.g., Cornwall & Hurd, 2015). Our findings suggest that, in some regions, OA metric changes in subsurface waters with weaker buffering can be significantly larger than surface changes (which may exhibit similar relative changes; Figure S19 in Supporting Information S1), indicating that experimental conditions thought to represent the distant future for the surface ocean may also represent a not-so-distant future for deeper layers of the water column. In addition to mean state considerations, Arroyo et al. (2022) determined that North Pacific waters with amplified subsurface OA changes regularly bathe the continental shelf during upwelling events in the California Current Large Marine Ecosystem (CCLME). Thus, the seasonal range of OA metric extremes on the shelf of the CCLME may have increased by significantly more than in overlying surface waters since the preindustrial period. Inverting the perception that OA impacts attenuate with depth may provide useful new context when designing OA laboratory experiments and interpreting relationships between organismal plasticity and environmental variability (e.g., Vargas et al., 2022).

The nonlinear amplification of interior ocean $p\mathrm{CO_2}$ changes associated with C_{ant} accumulation may have implications for anthropogenic carbon storage in the ocean. C_{ant} enters the ocean due to persistent growth in atmospheric $p\mathrm{CO_2}$ (presently ∼2.5 μatm yr^{-1}) that in turn causes persistent growth in surface ocean $p\mathrm{CO_2}$ at a rate that largely tracks the atmosphere; therefore, changes in sea-air $p\mathrm{CO_2}$ disequilibrium ($\Delta p\mathrm{CO_{2\ Sea\text{-}Air}}$) have occurred gradually (McKinley et al., 2017). The re-emergence of subsurface waters that have experienced $p\mathrm{CO_2}$ changes >100% larger than global surface ocean changes (Figure S5 in Supporting Information S1) could greatly increase the rate of $\mathrm{CO_2}$ evasion during water mass ventilation. In areas where water masses do not fully equilibrate with the atmosphere prior to subduction (e.g., the Southern Ocean), changes in the rate of $\mathrm{CO_2}$ evasion from the ocean could influence the level of sea-air equilibration reached and thus the amount and efficiency of carbon stored (Eggleston & Galbraith, 2018; Ito & Follows, 2013). With international goals to reduce atmospheric $\mathrm{CO_2}$ levels and eventually achieve net-zero $\mathrm{CO_2}$ emissions (International Energy Agency, 2021), this raises the question: where and when will waters experiencing amplified subsurface $p\mathrm{CO_2}$ changes re-emerge, and could this meaningfully impact ocean carbon storage efficiency?

While we have focused on the chemical changes associated with OA, the same concepts hold for other scenarios in which interior ocean carbon or alkalinity gradients are modified; as is the case for many mCDR strategies (National Academies of Sciences, Engineering, and Medicine, 2022). The efficacy and environmental implications of mCDR strategies will be depth-dependent for some key OA metrics. Like the RF, the Alkalinity sensitivity Factor (AF; Takahashi et al., 1993) describes the relative change in $p\mathrm{CO_2}$ associated with a relative change in TA, assuming all other variables are held constant. The AF is elevated at depth so that $p\mathrm{CO_2}$ is more sensitive to alkalinity addition below the surface (Figure S20). This enhanced sensitivity coupled with natural calcium carbonate dissolution (Figure S7) helps to partially compensate for $p\mathrm{CO_2}$ increases resulting from the remineralization of organic matter; however, there is much more carbon added through remineralization than calcium carbonate dissolution (Figure S6). While surface ocean alkalinity enhancement has largely been considered an mCDR strategy to mitigate climate change with the potential co-benefit of OA mitigation, the intentional addition of alkalinity below the surface could mitigate OA impacts that may be more deleterious than previously realized. As these waters will eventually return to the sea surface, mitigating extreme subsurface OA impacts could preemptively mitigate some of the most extreme surface OA impacts as well. Subsurface alkalinity addition could also mitigate future ocean-based $\mathrm{CO_2}$ emissions in regions where subsurface waters with large, C_{ant}-induced $p\mathrm{CO_2}$ perturbations are expected to re-emerge at the sea surface, such as eastern boundary upwelling regions or obduction hot spots. Some of the most abundant mineral sources of TA (e.g., carbonate minerals; Caserini et al., 2022) being considered for use in mCDR do not readily dissolve in modern surface ocean conditions (Kheshgi, 1995) but could dissolve while sinking through undersaturated portions of the water column (Figure 4).

This is commonly viewed as efficiency loss for mCDR. However, we show that the resulting mitigation of interior OA, and the potential for reductions in future ocean-based CO_2 emissions, could be disproportionately impactful.

5. Conclusions

The accumulation of anthropogenic carbon (C_{ant}) in the ocean interior has resulted in subsurface (>100 m) pCO_2, RF, and [H^+] changes that significantly exceeded their respective surface change magnitudes, sometimes by >100%. These amplified subsurface changes can predominantly be attributed to nonlinear carbonate chemistry effects in weakly buffered waters that have experienced a significant amount of organic matter remineralization. Under these conditions, pCO_2, RF, and [H^+] have a stronger response to carbon addition than they do at the sea surface. Such subsurface amplified signals are not yet consistently discernible for pH within the GLODAPv2.2016b mapped product but may be anticipated, as nonlinear carbonate chemistry effects are also working to amplify the subsurface pH response to C_{ant} accumulation (Figure S11a–S11c in Supporting Information S1). C_{ant}-induced changes in Ω_{Ar} are surface intensified, and are expected to remain so with C_{ant} accumulation because nonlinear carbonate chemistry effects weakly mitigate Ω_{Ar} declines at depth. Further work is needed to evaluate how subsurface carbonate chemistry has changed and will continue to change beyond the year 2002, and what this could mean for ocean ecosystems that are under pressure from a variety of anthropogenic stressors, which may eventually include the impacts of mCDR. Determining where and when subsurface waters with large C_{ant}-induced pCO_2 changes could meaningfully impact future ocean-based CO_2 emissions will be valuable for understanding marine carbon cycle feedbacks and developing informed ocean-based emissions reduction and negative emissions strategies.

Data Availability Statement

All data used in this study are publicly available. The GLODAPv2.2016b mapped data product is available through NOAA's National Centers for Environmental Information: https://www.nodc.noaa.gov/archive/arc0107/0162565/2.2/data/0-data/mapped/. Preformed property estimates based on GLODAPv2 data are available through Zenodo: https://zenodo.org/record/3745002. The GOSML mixed layer climatology product is available at: https://www.pmel.noaa.gov/gosml/. Water mass ages based on GLODAPv2 data are available through NCEI: https://www.ncei.noaa.gov/data/oceans/ncei/ocads/metadata/0226793.html.

Acknowledgments
The authors thank the many scientists who contributed to the GLODAPv2 database (www.glodap.info) by securing funding, dedicating their time to collect and share data, and assembling and quality-controlling those data. AJF was supported by NOAA's Pacific Marine Environmental Laboratory (PMEL). BRC, JDS, and HF were funded through the Cooperative Institute for Climate, Ocean, and Ecosystem Studies (CICOES) under NOAA Cooperative Agreement NA20OAR4320271 and supported by NOAA's PMEL. BRC thanks Kathy Tedesco of NOAA's Global Ocean Monitoring and Observations Program for supporting the Carbon Data Management and Synthesis Grant, which funded his contributions to this project (Fund Ref No. 100007298). MCA was supported by the Eugene Cota-Robles Fellowship administered by UCSC and the NOAA OA Program (Grant NA19OAR0170357). YH was supported by the National Science Foundation (Award No. 2032754) and NOAA PMEL. This is PMEL contribution 5504 and CICOES contribution 2023-1267.

References

Anderson, L. A., & Sarmiento, J. L. (1994). Redfield ratios of remineralization determined by nutrient data analysis. *Global Biogeochemical Cycles*, *8*(1), 65–80. https://doi.org/10.1029/93GB03318

Arroyo, M. C., Fassbender, A. J., Carter, B. R., Edwards, C. A., Fiechter, J., Norgaard, A., & Feely, R. A. (2022). Dissimilar sensitivities of Ocean Acidification metrics to anthropogenic carbon accumulation in the central North Pacific Ocean and California current large marine ecosystem. *Geophysical Research Letters*, *49*(15), 1–12. https://doi.org/10.1029/2022GL097835

Bach, L. T. (2015). Reconsidering the role of carbonate ion concentration in calcification by marine organisms. *Biogeosciences*, *12*(16), 4939–4951. https://doi.org/10.5194/bg-12-4939-2015

Bates, N., Astor, Y., Church, M. J., Currie, K., Dore, J., González-Dávila, M., et al. (2014). A time-series view of changing ocean chemistry due to ocean uptake of anthropogenic CO_2 and ocean acidification. *Oceanography*, *27*(1), 126–141. https://doi.org/10.5670/oceanog.2014.16

Bianchi, G. & Skjoldal, H. R. (Eds.) (2008)., *The ecosystem approach to fisheries*. Food and Agriculture Organization of the United Nations. Retrieved from https://onlinelibrary.wiley.com/doi/abs/10.1111/j.1095-8649.2009.02440_6.x

Boyd, P. W., Cornwall, C. E., Davison, A., Doney, S. C., Fourquez, M., Hurd, C. L., et al. (2016). Biological responses to environmental heterogeneity under future ocean conditions. *Global Change Biology*, *22*(8), 1–18. https://doi.org/10.1111/gcb.13287

Breitburg, D., Levin, L. A., Oschlies, A., Grégoire, M., Chavez, F. P., Conley, D. J., et al. (2018). Declining oxygen in the global ocean and coastal waters. *Science*, *359*(6371), eaam7240. https://doi.org/10.1126/science.aam7240

Broecker, W. S., Takahashi, T., Simpson, H. J. J., & Peng, T.-H.-H. (1979). Fate of fossil fuel carbon dioxide and the global carbon budget. *Science*, *206*(4417), 409–418. https://doi.org/10.1126/science.206.4417.409

Byrne, R. H., Mecking, S., Feely, R. A., & Liu, X. (2010). Direct observations of basin-wide acidification of the North Pacific Ocean. *Geophysical Research Letters*, *37*(2), 1–5. https://doi.org/10.1029/2009GL040999

Caldeira, K., & Wickett, M. E. (2003). Anthropogenic carbon and ocean pH. *Nature*, *425*(6956), 365. https://doi.org/10.1038/425365a

Carter, B. R., Feely, R. A., Lauvset, S. K., Olsen, A., DeVries, T., & Sonnerup, R. (2021). Preformed properties for marine organic matter and carbonate mineral cycling quantification. *Global Biogeochemical Cycles*, *35*(1). https://doi.org/10.1029/2020GB006623

Carter, B. R., Feely, R. A., Wanninkhof, R. H., Kouketsu, S., Sonnerup, R. E., Pardo, P. C., et al. (2019). Pacific anthropogenic carbon between 1991 and 2017. *Global Biogeochemical Cycles*, *33*(5), 597–617. https://doi.org/10.1029/2018GB006154

Carter, B. R., Feely, R. A., Williams, N. L., Dickson, A. G., Fong, M. B., & Takeshita, Y. (2017). Updated methods for global locally interpolated estimation of alkalinity, pH, and nitrate. *Limnology and Oceanography: Methods*, *16*(2), 119–131. https://doi.org/10.1002/lom3.10232

Caserini, S., Storni, N., & Grosso, M. (2022). The availability of limestone and other raw materials for ocean alkalinity enhancement. *Global Biogeochemical Cycles*, *36*(5), e2021GB007246. https://doi.org/10.1029/2021GB007246

19449224, 2023, 12, Downloaded from https://agupubs.onlinelibrary.wiley.com/doi/10.1029/2023GB007843 by Ifremer Centre Bretagne Blp, Wiley Online Library on [06/03/2025]. See the Terms and Conditions (https://onlinelibrary.wiley.com/terms-and-conditions) on Wiley Online Library for rules of use; OA articles are governed by the applicable Creative Commons License

19449224, 2023, 12, Downloaded from https://agupubs.onlinelibrary.wiley.com/doi/10.1029/2023GB007843 by Ifremer Centre Bretagne Blp, Wiley Online Library on [06/03/2025]. See the Terms and Conditions (https://onlinelibrary.wiley.com/terms-and-conditions) on Wiley Online Library for rules of use; OA articles are governed by the applicable Creative Commons License

Cassar, N., Nicholson, D., Khatiwala, S., & Cliff, E. (2021). Decomposing the oxygen signal in the ocean interior: Beyond decomposing organic matter. *Geophysical Research Letters*, *48*(18), 1–12. https://doi.org/10.1029/2021GL092621

Chen, C.-T. A., Lui, H.-K., Hsieh, C.-H., Yanagi, T., Kosugi, N., Ishii, M., & Gong, G.-C. (2017). Deep oceans may acidify faster than anticipated due to global warming. *Nature Climate Change*, *7*(12), 890–894. https://doi.org/10.1038/s41558-017-0003-y

Chen, H., Haumann, F. A., Talley, L. D., Johnson, K. S., & Sarmiento, J. L. (2022). The deep ocean's carbon exhaust. *Global Biogeochemical Cycles*, *36*(7), 1–21. https://doi.org/10.1029/2021GB007156

Clements, J. C., & Hunt, H. L. (2015). Marine animal behaviour in a high CO_2 ocean. *Marine Ecology Progress Series*, *536*, 259–279. https://doi.org/10.3354/meps11426

Cooley, S. R., & Doney, S. C. (2009). Anticipating ocean acidification's economic consequences for commercial fisheries. *Environmental Research Letters*, *4*(2), 024007. https://doi.org/10.1088/1748-9326/4/2/024007

Cornwall, C. E., & Hurd, C. L. (2015). Experimental design in ocean acidification research: Problems and solutions. *ICES Journal of Marine Science: Journal Du Conseil*, *73*(December), fsv118–581. https://doi.org/10.1093/icesjms/fsv118

Deutsch, C., Penn, J. L., & Seibel, B. (2020). Metabolic trait diversity shapes marine biogeography. *Nature*, *585*(7826), 557–562. https://doi.org/10.1038/s41586-020-2721-y

DeVries, T. (2014). The oceanic anthropogenic CO_2 sink: Storage, air-sea fluxes, and transports over the industrial era. *Global Biogeochemical Cycles*, *28*(7), 631–647. https://doi.org/10.1002/2013GB004739

DeVries, T. (2022). The Ocean carbon cycle. *Annual Review of Environment and Resources*, *47*(1), 317–341. https://doi.org/10.1146/annurev-environ-120920-111307

Dickson, A. G., Wesolowski, D. J., Palmer, D. A., & Mesmer, R. E. (1990). Dissociation constant of bisulfate ion in aqueous sodium chloride solutions to 250°C. *Journal of Physical Chemistry*, *94*(20), 7978–7985. https://doi.org/10.1021/j100383a042

Doney, S. C., Busch, D. S., Cooley, S. R., & Kroeker, K. J. (2020). The impacts of Ocean Acidification on marine ecosystems and reliant human communities. *Annual Review of Environment and Resources*, *45*(1), 83–112. https://doi.org/10.1146/annurev-environ-012320-083019

Doney, S. C., Lima, I., Feely, R. A., Glover, D. M., Lindsay, K., Mahowald, N., et al. (2009). Mechanisms governing interannual variability in upper-ocean inorganic carbon system and air–sea CO_2 fluxes: Physical climate and atmospheric dust. *Deep Sea Research Part II: Topical Studies in Oceanography*, *56*(8–10), 640–655. https://doi.org/10.1016/j.dsr2.2008.12.006

Dore, J., Lukas, R., Sadler, D. W., Church, M. J., & Karl, D. M. (2009). Physical and biogeochemical modulation of ocean acidification in the central North Pacific. *Proceedings of the National Academy of Sciences of the United States of America*, *106*(30), 12235–12240. https://doi.org/10.1073/pnas.0906044106

Eggleston, S., & Galbraith, E. D. (2018). The devil's in the disequilibrium: Multi-component analysis of dissolved carbon and oxygen changes under a broad range of forcings in a general circulation model. *Biogeosciences*, *15*(12), 3761–3777. https://doi.org/10.5194/bg-2017-328

Egleston, E. S., Sabine, C. L., & Morel, F. M. M. (2010). Revelle revisited: Buffer factors that quantify the response of ocean chemistry to changes in DIC and alkalinity. *Global Biogeochemical Cycles*, *24*(1), 1–9. https://doi.org/10.1029/2008GB003407

Esbaugh, A. J. (2018). Physiological implications of ocean acidification for marine fish: Emerging patterns and new insights. *Journal of Comparative Physiology B: Biochemical, Systemic, and Environmental Physiology*, *188*(1), 1–13. https://doi.org/10.1007/s00360-017-1105-6

Fassbender, A. J., Orr, J. C., & Dickson, A. G. (2021). Technical note: Interpreting pH changes. *Biogeosciences*, *18*(4), 1407–1415. https://doi.org/10.5194/bg-18-1407-2021

Fassbender, A. J., Sabine, C. L., & Palevsky, H. I. (2017). Nonuniform ocean acidification and attenuation of the ocean carbon sink. *Geophysical Research Letters*, *44*(16), 8404–8413. https://doi.org/10.1002/2017GL074389

Fay, A. R., & McKinley, G. A. (2013). Global trends in surface ocean pCO_2 from in situ data. *Global Biogeochemical Cycles*, *27*(2), 541–557. https://doi.org/10.1002/gbc.20051

Feely, R. A., Doney, S. C., & Cooley, S. R. (2009). Ocean acidification: Present conditions and future changes in a high-CO_2 world. *Oceanography*, *22*(4), 36–47. https://doi.org/10.5670/oceanog.2009.95

Feely, R. A., Okazaki, R. R., Cai, W.-J., Bednaršek, N., Alin, S. R., Byrne, R. H., & Fassbender, A. (2018). The combined effects of acidification and hypoxia on pH and aragonite saturation in the coastal waters of the California current ecosystem and the northern Gulf of Mexico. *Continental Shelf Research*, *152*(July), 50–60. https://doi.org/10.1016/j.csr.2017.11.002

Feely, R. A., Sabine, C. L., Lee, K., Berelson, W. M., Kleypas, J., Fabry, V. J., & Millero, F. J. J. (2004). Impact of anthropogenic CO_2 on the $CaCO_3$ system in the oceans. *Science (New York, N.Y.)*, *305*(5682), 362–366. https://doi.org/10.1126/science.1097329

Fjeld, K., Tiller, R., Grimaldo, E., Grimsmo, L., & Standal, I.-B. (2023). Mesopelagics–New gold rush or castle in the sky? *Marine Policy*, *147*, 105359. https://doi.org/10.1016/j.marpol.2022.105359

Fletcher, W. J., Shaw, J., Metcalf, S. J., & Gaughan, D. J. (2010). An ecosystem based fisheries management framework: The efficient, regional-level planning tool for management agencies. *Marine Policy*, *34*(6), 1226–1238. https://doi.org/10.1016/j.marpol.2010.04.007

Friedlingstein, P., Jones, M. W., O'Sullivan, M., Andrew, R. M., Bakker, D. C. E., Hauck, J., et al. (2022). Global carbon budget 2021. *Earth System Science Data*, *14*(4), 1917–2005. https://doi.org/10.5194/essd-14-1917-2022

Garcia, S. M., & Cochrane, K. L. (2005). Ecosystem approach to fisheries: A review of implementation guidelines. *ICES Journal of Marine Science*, *62*(3), 311–318. https://doi.org/10.1016/j.icesjms.2004.12.003

Gattuso, J.-P., Epitalon, J.-M., & Orr, J. (2020). seacarb: Seawater carbonate chemistry. (Version 3.2.13). Retrieved from https://CRAN.R-project.org/package=seacarb

Gruber, N., Clement, D., Carter, B. R., Feely, R. A., van Heuven, S. M. A. C., Hoppema, M., et al. (2019). The oceanic sink for anthropogenic CO_2 from 1994 to 2007. *Science*, *363*(6432), 1193–1199. https://doi.org/10.1126/science.aau5153

Guinotte, J. M., & Fabry, V. J. (2008). Ocean acidification and its potential effects on marine ecosystems. *Annals of the New York Academy of Sciences*, *1134*(1), 320–342. https://doi.org/10.1196/annals.1439.013

Hamme, R. C., Nicholson, D. P., Jenkins, W. J., & Emerson, S. R. (2019). Using noble gases to assess the ocean's carbon pumps. *Annual Review of Marine Science*, *11*(1), 75–103. https://doi.org/10.1146/annurev-marine-121916-063604

Hedges, J. I., Baldock, J. A., Gélinas, Y., Lee, C., Peterson, M. L., & Wakeham, S. G. (2002). The biochemical and elemental compositions of marine plankton: A NMR perspective. *Marine Chemistry*, *78*(1), 47–63. https://doi.org/10.1016/S0304-4203(02)00009-9

Henderikx Freitas, F., White, A. E., & Quay, P. D. (2020). Diel measurements of oxygen- and carbon-based ocean metabolism across a trophic gradient in the North Pacific. *Global Biogeochemical Cycles*, *34*(11), e2019GB006518. https://doi.org/10.1029/2019GB006518

Heuer, R. M., & Grosell, M. (2014). Physiological impacts of elevated carbon dioxide and ocean acidification on fish. *American Journal of Physiology - Regulatory, Integrative and Comparative Physiology*, *307*(9), R1061–R1084. https://doi.org/10.1152/ajpregu.00064.2014

Howard, E. M., Penn, J. L., Frenzel, H., Seibel, B. A., Bianchi, D., Renault, L., et al. (2020). Climate-driven aerobic habitat loss in the California Current System. *Science Advances*, *6*(20), eaay3188. https://doi.org/10.1126/sciadv.aay3188

19449224, 2023, 12, Downloaded from https://agupubs.onlinelibrary.wiley.com/doi/10.1029/2023GB007843 by Ifremer Centre Bretagne Blp, Wiley Online Library on [06/03/2025]. See the Terms and Conditions (https://onlinelibrary.wiley.com/terms-and-conditions) on Wiley Online Library for rules of use; OA articles are governed by the applicable Creative Commons License

Humphreys, M. P., Lewis, E. R., Sharp, J. D., & Pierrot, D. (2022). PyCO2SYS v1.8: Marine carbonate system calculations in Python. *Geoscientific Model Development*, *15*(1), 15–43. https://doi.org/10.5194/gmd-15-15-2022

Iida, Y., Takatani, Y., Kojima, A., & Ishii, M. (2021). Global trends of ocean CO_2 sink and ocean acidification: An observation-based reconstruction of surface ocean inorganic carbon variables. *Journal of Oceanography*, *77*(2), 323–358. https://doi.org/10.1007/s10872-020-00571-5

International Energy Agency. (2021). Net zero by 2050: A roadmap for the global energy sector. Retrieved from https://www.iea.org/reports/net-zero-by-2050

Ito, T., & Follows, M. J. (2013). Air-sea disequilibrium of carbon dioxide enhances the biological carbon sequestration in the Southern Ocean. *Global Biogeochemical Cycles*, *27*(4), 1129–1138. https://doi.org/10.1002/2013GB004682

Iudicone, D., Rodgers, K. B., Plancherel, Y., Aumont, O., Ito, T., Key, R. M., et al. (2016). *The formation of the ocean's anthropogenic carbon reservoir* (pp. 1–16). Nature Publishing Group. https://doi.org/10.1038/srep35473

Jeansson, E., Steinfeldt, R., & Tanhua, T. (2021). *Water mass ages based on GLODAPv2 data product (NCEI Accession 0226793). Mean age calculated from SF6 and the TTD method in years*. NOAA National Centers for Environmental Information. https://doi.org/10.25921/xp33-q351

Jiang, L.-Q., Carter, B. R., Feely, R. A., Lauvset, S. K., & Olsen, A. (2019). Surface ocean pH and buffer capacity: Past, present and future. *Scientific Reports*, *9*(1), 18624. https://doi.org/10.1038/s41598-019-55039-4

Jiang, L.-Q., Dunne, J., Carter, B. R., Tjiputra, J. F., Terhaar, J., Sharp, J. D., et al. (2023). Global surface Ocean Acidification indicators from 1750 to 2100. *Journal of Advances in Modeling Earth Systems*, *15*(3), e2022MS003563. https://doi.org/10.1029/2022MS003563

Jiang, L.-Q., Feely, R. A., Carter, B. R., Greeley, D. J., Gledhill, D. K., & Arzayus, K. M. (2015). Climatological distribution of aragonite saturation state in the global oceans. *Global Biogeochemical Cycles*, *29*(10), 1656–1673. https://doi.org/10.1002/2015GB005198

Johnson, G. C., & Lyman, J. M. (2022). GOSML: A Global Ocean surface mixed layer statistical monthly climatology: Means, percentiles, skewness, and kurtosis. *Journal of Geophysical Research: Oceans*, *127*(1). https://doi.org/10.1029/2021JC018219

Key, R. M., Kozyr, A., Sabine, C. L., Lee, K., Wanninkhof, R., Bullister, J. L., et al. (2004). A global ocean carbon climatology: Results from global data analysis project (GLODAP). *Global Biogeochemical Cycles*, *18*(4), 1–23. https://doi.org/10.1029/2004GB002247

Key, R. M., Olsen, A., van Heuven, S., Lauvset, S. K., Velo, A., Lin, X., et al. (2015). Global Ocean data analysis project. Version 2 (GLODAPv2) [Other]. https://doi.org/10.3334/CDIAC/OTG

Khatiwala, S., Tanhua, T., Mikaloff Fletcher, S., Gerber, M., Doney, S. C., Graven, H. D., et al. (2013). Global ocean storage of anthropogenic carbon. *Biogeosciences*, *10*(4), 2169–2191. https://doi.org/10.5194/bg-10-2169-2013

Kheshgi, H. S. (1995). Sequestering atmospheric carbon dioxide by increasing ocean alkalinity. *Energy*, *20*(9), 915–922. https://doi.org/10.1016/0360-5442(95)00035-F

Kourantidou, M., & Jin, D. (2022). Mesopelagic–epipelagic fish nexus in viability and feasibility of commercial-scale mesopelagic fisheries. *Natural Resource Modeling*, *35*(4), e12350. https://doi.org/10.1111/nrm.12350

Kwiatkowski, L., & Orr, J. C. (2018). Diverging seasonal extremes for ocean acidification during the twenty-first century. *Nature Climate Change*, *8*(2), 141–145. https://doi.org/10.1038/s41558-017-0054-0

Kwiatkowski, L., Torres, O., Bopp, L., Aumont, O., Chamberlain, M., Christian, J. R., et al. (2020). Twenty-first century ocean warming, acidification, deoxygenation, and upper-ocean nutrient and primary production decline from CMIP6 model projections. *Biogeosciences*, *17*(13), 3439–3470. https://doi.org/10.5194/bg-17-3439-2020

Lauvset, S. K., Carter, B. R., Pèrez, F. F., Jiang, L.-Q., Feely, R. A., Velo, A., & Olsen, A. (2020). Processes driving global interior ocean pH distribution. *Global Biogeochemical Cycles*, *34*(1), 1–17. https://doi.org/10.1029/2019GB006229

Lauvset, S. K., Gruber, N., Landschützer, P., Olsen, A., & Tjiputra, J. (2015). Trends and drivers in global surface ocean pH over the past 3 decades. *Biogeosciences*, *12*(5), 1285–1298. https://doi.org/10.5194/bg-12-1285-2015

Lauvset, S. K., Key, R. M., Olsen, A., van Heuven, S. M. A. C., Velo, A., Lin, X., et al. (2016). A new global interior ocean mapped climatology: The 1° × 1° GLODAP version 2. *Earth System Science Data*, *8*(2), 325–340. https://doi.org/10.5194/essd-8-325-2016

Lee, K., Kim, T.-W., Byrne, R. H., Millero, F. J., Feely, R. A., & Liu, Y.-M. (2010). The universal ratio of boron to chlorinity for the North Pacific and North Atlantic oceans. *Geochimica et Cosmochimica Acta*, *74*(6), 1801–1811. https://doi.org/10.1016/j.gca.2009.12.027

Lewis, E., & Wallace, D. W. R. (1998). Program developed for CO_2 system calculations. *Carbon Dioxide Information Analysis Center, Oak Ridge National Laboratory, U.S. Department of Energy, Oak Ridge, Tennessee. Environmental Sciences Division. Publication No. 4735*. Oak Ridge TN, Oak Ridge National Laboratory Environmental Sciences Division, v. 4735.

Lindsay, K., Bonan, G. B., Doney, S. C., Hoffman, F. M., Lawrence, D. M., Long, M. C., et al. (2014). Preindustrial-control and twentieth-century carbon cycle experiments with the Earth system model CESM1(BGC). *Journal of Climate*, *27*(24), 8981–9005. https://doi.org/10.1175/JCLI-D-12-00565.1

Lotze, H. K., Tittensor, D. P., Bryndum-Buchholz, A., Eddy, T. D., Cheung, W. W. L., Galbraith, E. D., et al. (2019). Global ensemble projections reveal trophic amplification of ocean biomass declines with climate change. *Proceedings of the National Academy of Sciences*, *116*(26), 12907–12912. https://doi.org/10.1073/pnas.1900194116

Lueker, T. J., Dickson, A. G., & Keeling, C. D. (2000). Ocean pCO2 calculated from dissolved inorganic carbon, alkalinity, and equations for K1 and K2: Validation based on laboratory measurements of CO2 in gas and seawater at equilibrium. *Marine Chemistry*, *70*(1–3), 105–119. https://doi.org/10.1016/S0304-4203(00)00022

Marshall, K. N., Koehn, L. E., Levin, P. S., Essington, T. E., & Jensen, O. P. (2019). Inclusion of ecosystem information in US fish stock assessments suggests progress toward ecosystem-based fisheries management. *ICES Journal of Marine Science*, *76*(1), 1–9. https://doi.org/10.1093/icesjms/fsy152

McKinley, G. A., Fay, A. R., Lovenduski, N. S., & Pilcher, D. J. (2017). Natural variability and anthropogenic trends in the ocean carbon sink. *Annual Review of Marine Science*, *9*(1), 125–150. https://doi.org/10.1146/annurev-marine-010816-060529

McNeil, B. I., & Sasse, T. P. (2016). Future ocean hypercapnia driven by anthropogenic amplification of the natural CO_2 cycle. *Nature*, *529*(7586), 383–386. https://doi.org/10.1038/nature16156

Middelburg, J. J., Soetaert, K., & Hagens, M. (2020). Ocean alkalinity, buffering and biogeochemical processes. *Reviews of Geophysics*, *58*(3). https://doi.org/10.1029/2019RG000681

Moreno, A. R., Garcia, C. A., Larkin, A. A., Lee, J. A., Wang, W., Moore, J. K., et al. (2020). Latitudinal gradient in the respiration quotient and the implications for ocean oxygen availability. *Proceedings of the National Academy of Sciences*, *117*(37), 202004986–202022872. https://doi.org/10.1073/pnas.2004986117

Moreno, A. R., Larkin, A. A., Lee, J. A., Gerace, S. D., Tarran, G. A., & Martiny, A. C. (2022). Regulation of the respiration quotient across ocean basins. *AGU Advances*, *3*(5), e2022AV000679. https://doi.org/10.1029/2022AV000679

Müller, J. D. (2023). RECCAP2-ocean data collection [Dataset]. Zenodo. https://doi.org/10.5281/zenodo.7990823

National Academies of Sciences, Engineering, and Medicine. (2022). *A research strategy for ocean-based carbon dioxide removal and sequestration*. National Academies Press. 26278. https://doi.org/10.17226/26278

Negrete-García, G., Lovenduski, N. S., Hauri, C., Krumhardt, K. M., & Lauvset, S. K. (2019). Sudden emergence of a shallow aragonite saturation horizon in the Southern Ocean. *Nature Climate Change*, *9*(4), 313–317. https://doi.org/10.1038/s41558-019-0418-8

Nilsson, G. E., Dixson, D. L., Domenici, P., McCormick, M. I., Sørensen, C., Watson, S.-A., & Munday, P. L. (2012). Near-future carbon dioxide levels alter fish behaviour by interfering with neurotransmitter function. *Nature Climate Change*, *2*(3), 201–204. https://doi.org/10.1038/nclimate1352

Olsen, A., Key, R. M., Heuven, S. V., Lauvset, S. K., Velo, A., Lin, X., et al. (2016). The Global Ocean data analysis project version 2 (GLODAPv2) – An internally consistent data product for the world ocean. *Earth System Science Data*, *8*, 297–323. https://doi.org/10.5194/essd-8-297-2016

Orr, J. C., & Epitalon, J. M. (2015). Improved routines to model the ocean carbonate system: Mocsy 2.0. *Geoscientific Model Development*, *8*(3), 485–499. https://doi.org/10.5194/gmd-8-485-2015

Orr, J. C., Epitalon, J.-M., Dickson, A. G., & Gattuso, J.-P. (2018). Routine uncertainty propagation for the marine carbon dioxide system. *Marine Chemistry*, *207*, 84–107. https://doi.org/10.1016/j.marchem.2018.10.006

Orr, J. C., Epitalon, J.-M., & Gattuso, J.-P. (2015). Comparison of ten packages that compute ocean carbonate chemistry. *Biogeosciences*, *12*(5), 1483–1510. https://doi.org/10.5194/bg-12-1483-2015

Orr, J. C., Fabry, V. J., Aumont, O., Bopp, L., Doney, S. C., Feely, R. A., et al. (2005). Anthropogenic ocean acidification over the twenty-first century and its impact on calcifying organisms. *Nature*, *437*(7059), 681–686. https://doi.org/10.1038/nature04095

Oschlies, A., Brandt, P., Stramma, L., & Schmidtko, S. (2018). Drivers and mechanisms of ocean deoxygenation. *Nature Geoscience*, *11*(7), 467–473. https://doi.org/10.1038/s41561-018-0152-2

Perez, F. F., & Fraga, F. (1987). Association constant of fluoride and hydrogen ions in seawater. *Marine Chemistry*, *21*(2), 161–168. https://doi.org/10.1016/0304-4203(87)90036-3

Perry, S. F., & Gilmour, K. M. (2006). Acid–base balance and CO_2 excretion in fish: Unanswered questions and emerging models. *Respiratory Physiology & Neurobiology*, *154*(1), 199–215. https://doi.org/10.1016/j.resp.2006.04.010

Pikitch, E. K., Santora, C., Babcock, E. A., Bakun, A., Bonfil, R., Conover, D. O., et al. (2004). Ecosystem-based fishery management. *Science*, *305*(5682), 346–347. https://doi.org/10.1126/science.1098222

Revelle, R., & Suess, H. E. (1957). Carbon dioxide exchange between atmosphere and ocean and the question of an increase of atmospheric CO_2 during the past decades. *Tellus*, *9*(1), 18–27. https://doi.org/10.1111/j.2153-3490.1957.tb01849.x

Sabine, C. L., Feely, R. A., Gruber, N., Key, R. M., Lee, K., Bullister, J. L., et al. (2004). The oceanic sink for anthropogenic CO_2. *Science*, *305*(5682), 367–371. https://doi.org/10.1126/science.1097403

Sarmiento, J. L., & Gruber, N. (2006). *Ocean biogeochemical dynamics*. Princeton University Press.

Sharp, J. D., Pierrot, D., Humphreys, M. P., Epitalon, j.-M., Orr, J. C., Lewis, E. R., & Wallace, D. W. R. (2020). CO2SYSv3 for MATLAB. https://doi.org/10.5281/zenodo.4023039

Sundin, J. (2023). The effects of ocean acidification on fishes – History and future outlook. *Journal of Fish Biology*, *103*(4), 765–772. https://doi.org/10.1111/jfb.15323

Sutton, A. J., Feely, R. A., Maenner-Jones, S., Musielwicz, S., Osborne, J., Dietrich, C., et al. (2019). Autonomous seawater pCO_2 and pH time series from 40 surface buoys and the emergence of anthropogenic trends. *Earth System Science Data*, *11*(1), 421–439. https://doi.org/10.5194/essd-11-421-2019

Takahashi, T., Olafsson, J., Goddard, J. G., Chipman, D. W., & Sutherland, S. C. (1993). Seasonal variation of CO_2 and nutrients in the high-latitude surface oceans: A comparative study. *Global Biogeochemical Cycles*, *7*(4), 843–878. https://doi.org/10.1029/93GB02263

Takahashi, T., Sutherland, S. C., Chipman, D. W., Goddard, J. G., Ho, C., Newberger, T., et al. (2014). Climatological distributions of pH, pCO_2, total CO_2, alkalinity, and $CaCO_3$ saturation in the global surface ocean, and temporal changes at selected locations. *Marine Chemistry*, *164*, 95–125. https://doi.org/10.1016/j.marchem.2014.06.004

Tittensor, D. P., Novaglio, C., Harrison, C. S., Heneghan, R. F., Barrier, N., Bianchi, D., et al. (2021). Next-generation ensemble projections reveal higher climate risks for marine ecosystems. *Nature Climate Change*, *11*(11), 973–981. https://doi.org/10.1038/s41558-021-01173-9

van Heuven, S. M. A. C., Pierrot, D., Rae, J. W. B., Lewis, E., & Wallace, D. W. R. (2011). MATLAB program developed for CO_2 system calculations. In *ORNL/CDIAC-105b. Carbon dioxide information analysis Center, Oak Ridge National Laboratory, U.S. Department of Energy, Oak Ridge, Tennessee*. https://doi.org/10.3334/CDIAC/otg.CO2SYS_MATLAB_v1.1

Vargas, C. A., Cuevas, L. A., Broitman, B. R., San Martin, V. A., Lagos, N. A., Gaitán-Espitia, J. D., & Dupont, S. (2022). Upper environmental pCO_2 drives sensitivity to ocean acidification in marine invertebrates. *Nature Climate Change*, *12*(2), 200–207. https://doi.org/10.1038/s41558-021-01269-2

Volk, T., & Hoffert, M. I. (1985). Ocean carbon pumps: Analysis of relative strengths and efficiencies in ocean-driven atmospheric CO_2 changes. In E. T. Sundquist & W. S. Broecker (Eds.), *The carbon cycle and atmospheric CO_2: Natural variations Archean to present* (pp. 99–110). American Geophysical Union. Geophysical Monograph 32.

Weiss, R. F. (1974). Carbon dioxide in water and seawater: The solubility of a non-ideal gas. *Marine Chemistry*, *2*(3), 203–215. https://doi.org/10.1016/0304-4203(74)90015-2

Wolf-Gladrow, D. A., Zeebe, R. E., Klaas, C., Kortzinger, A., & Dickson, A. G. (2007). Total alkalinity: The explicit conservative expression and its application to biogeochemical processes. *Marine Chemistry*, *106*(1–2), 287–300. https://doi.org/10.1016/j.marchem.2007.01.006

Wu, Y., Hain, M. P., Humphreys, M. P., Hartman, S., & Tyrrell, T. (2019). What drives the latitudinal gradient in open-ocean surface dissolved inorganic carbon concentration? *Biogeosciences*, *16*(13), 2661–2681. https://doi.org/10.5194/bg-16-2661-2019

Yang, S., & Gruber, N. (2016). The anthropogenic perturbation of the marine nitrogen cycle by atmospheric deposition: Nitrogen cycle feedbacks and the 15N Haber-Bosch effect. *Global Biogeochemical Cycles*, *30*(10), 1418–1440. https://doi.org/10.1002/2016GB005421

Erratum

The originally published version of this article contained a few typographical errors in the supporting information. The errors have been corrected, and this may be considered the authoritative version of record.

19449224, 2023, 12, Downloaded from https://agupubs.onlinelibrary.wiley.com/doi/10.1029/2023GB007843 by Ifremer Centre Bretagne Blp, Wiley Online Library on [06/03/2025]. See the Terms and Conditions (https://onlinelibrary.wiley.com/terms-and-conditions) on Wiley Online Library for rules of use; OA articles are governed by the applicable Creative Commons License